Mechanisms of slope failure in Valles Marineris, Mars

D.P. Neuffer[1,2] & R.A. Schultz[1]

[1]Geomechanics-Rock Fracture Group, Department of Geological Sciences and Engineering/172, Mackay School of Earth Sciences and Engineering, University of Nevada, Reno, Nevada 89557-0138, United States
(e-mails: DPN@rtweng.com & schultz@mines.unr.edu)
[2]Now at: RTW Professional Engineers and Consultants, Inc., 825 Railroad St., Elko, NV 89801, United States

Abstract

The trough system of Valles Marineris, Mars contains numerous landslides in the large relief exposures (up to 8 km) of basaltic wall rock and soft interior layered deposits (ILDs). Eleven landslides, including eight circular failures, were mapped in the ILDs. Two wall rock landslide complexes and four ILD landslides were modelled using limit-equilibrium slope stability analysis to evaluate the mechanisms of slope failure. Wall rock landslide complexes in the Ophir and Hebes Chasmata required artesian fluid pressures of at least 41% of overburden pressure or ground accelerations of at least 0.19 Mars *g* for failure. Agreement between modelled and observed failure surface geometries and the difficulty of generating artesian pressures at a regional topographic high indicate that ground shaking from Marsquakes or impacts most likely triggered the modelled wall rock landslides. Triggering mechanisms, such as ground acceleration or fluid pressure, were also necessary for most other landslides in Valles Marineris wall rock. Given minimum rock mass strengths, ILD landslides in the Hebes and East Candor Chasmata did not require triggering mechanisms; thus, landslides in ILDs may be a result of gravitational, fluid, or seismic loading.

Keywords: earthquakes, landslides, pore pressure, rock mechanics, slope stability

Landslides were first identified in the walls of the equatorial trough system of Valles Marineris, Mars on images returned from the Mariner 9 mission (Sharp 1973). Subsequently, numerous workers have studied and analyzed landslides in Valles Marineris, but none have conclusively determined whether the slope failures were caused by forces other than gravity, and if so, which of the triggering forces were most significant. Two of the most common triggers of slope failure on Earth, fluid pressure changes and ground shaking (Wieczorek 1996), are also the most probable triggering mechanisms for landslides in Valles Marineris, Mars. Because landslides are some of the youngest and most pervasive features in the trough system, the involvement of fluids or seismicity in slope failure has important implications for the recent geological history of Mars. This work utilizes landslide mapping and slope stability analyses to evaluate the failure mechanisms of six landslides in central Valles Marineris, where exposures of interior layered deposits (ILDs) and wall rock are thickest and, hence, topographic relief is the greatest.

Valles Marineris forms an east–west trending trough system that extends approximately 4000 km across a region just south of the Martian equator (Fig. 1). Located immediately to the east of the Tharsis volcanic region, the Valles Marineris were formed by a combination of local subsidence and regional normal faulting (Schultz 1998a). The resulting trough walls display sequences of horizontal or shallow-dipping (McEwen *et al.* 1999; Fueten *et al.* 2005a), basalt flows *c.*5 to 50 m thick with total exposed thicknesses of up to 8 km (Fig. 2a) (McEwen *et al.* 1999). Locally, the layered basalt may be interbedded with mafic intrusives (Williams *et al.* 2003) or sedimentary rocks (Malin & Edgett 2000).

Simultaneous with or following the opening of Valles Marineris, sequences of layered materials were deposited in the chasmata (canyons), forming mound- and mesa-like landforms up to 6 km thick (Fig. 1) (Komatsu *et al.* 2004). Known as the ILDs, the mounds are comprised of light- to intermediate-toned beds ranging from a few metres to a few kilometres thick (Fig. 4a) (Malin & Edgett 2000); the beds have subhorizontal to *c.* 30° outward dipping attitudes depending on location (Lucchitta 2004; Hauber *et al.* 2005; Fueten *et al.* 2005b). Some ILD mounds have subhorizontal, dark- to intermediate-toned, resistant cap rock units with beds a few metres to a few hundred metres thick (Fig. 4a) (Lucchitta 1999; Malin & Edgett 2000; Komatsu *et al.* 2004; Hauber *et al.* 2005). In contrast to the spur and gully morphology displayed on wall slopes (Fig. 2a), ILD slopes show mostly fluted morphology (Fig. 4a) and are often separated from surrounding wall rock by large 'moats' (Fig. 1).

Hypotheses for the origin of the ILDs include lacustrine (e.g. McCauley 1978; Lucchitta 1982; Nedell *et al.* 1987; Komatsu *et al.* 1993; Weitz & Parker 2000; Malin & Edgett 2000), eolian (e.g. Peterson 1981), and volcanic (e.g. Peterson 1981; Lucchitta 1981; Witbeck *et al.* (1991); Komatsu *et al.* 1993; Weitz 1999) deposition. Other workers have proposed that the ILDs are subice volcanoes (e.g. Nedell *et al.* 1987; Croft 1990; Lucchitta *et al.* 1994) similar to those in Iceland (e.g. van Bemmelen & Rutten 1955; Jones 1969; Gudmundsson *et al.* 1997; Werner & Schmincke 1999), Antarctica (e.g. Smellie *et al.* 1993; Skilling 1994), Canada (e.g., Mathews 1947; Allen *et al.* 1982; Hickson *et al.* 1995), and Siberia (e.g. Komatsu *et al.* 2004); detailed observations of ILD stratigraphy, structure, and morphology by Chapman &

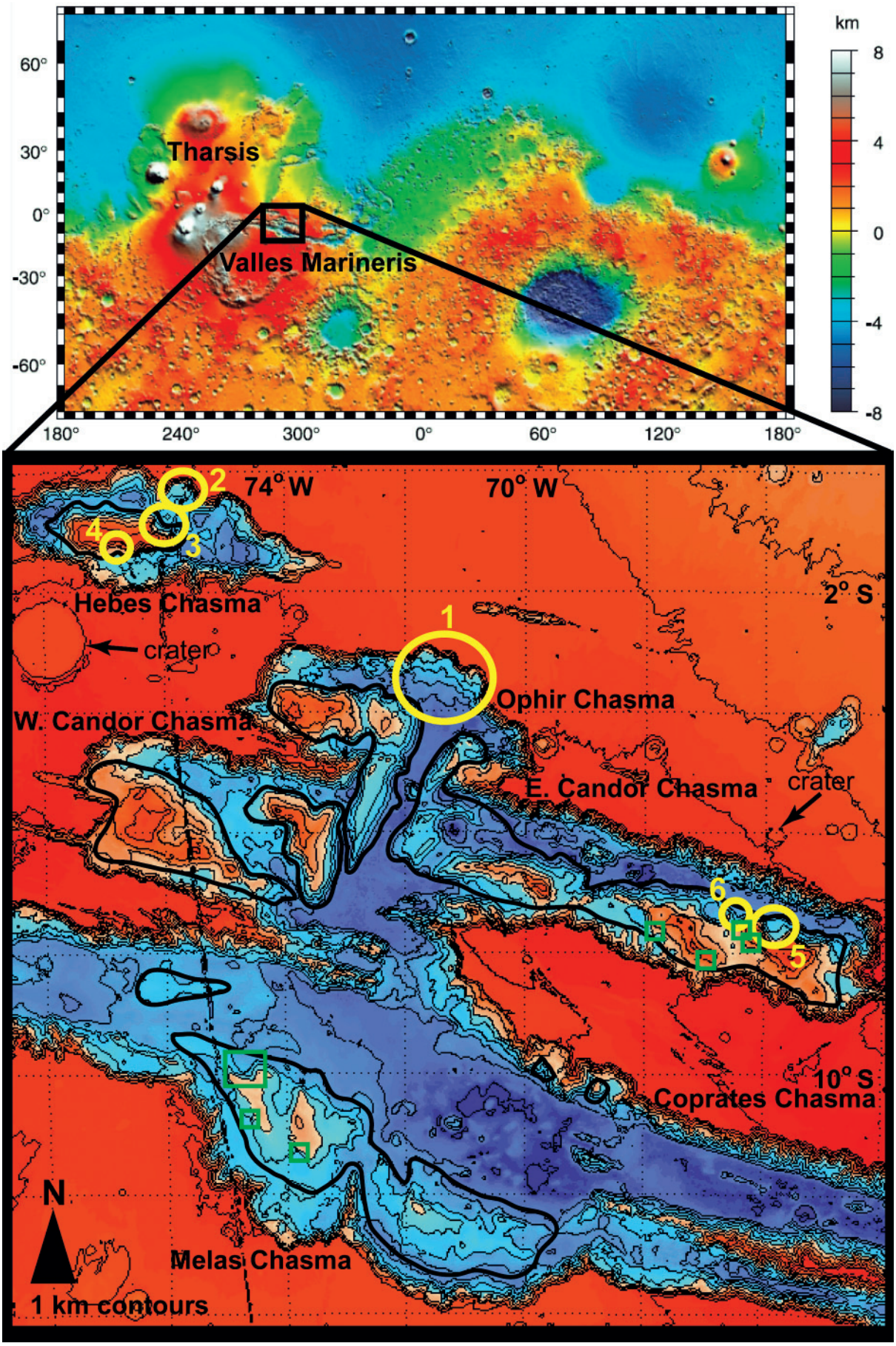
km
8
4
0
-4
-8
60°
30°
0°
-30°
-60°
180°
240°
300°
0°
60°
120°
180°
Tharsis
Valles Marineris
74° W
70° W
2° S
10° S
Hebes Chasma
crater
Ophir Chasma
W. Candor Chasma
E. Candor Chasma
crater
Coprates Chasma
Melas Chasma
N
1 km contours
1
2
3
4
5
6

Tanaka (2001) and Komatsu *et al.* (2004) support a subice or subaqueous volcanic origin for many ILDs. Clearly, a subglacial or lacustrine origin for the ILDs has significant consequences for the spatial and temporal distribution of water in the Valles Marineris region of Mars.

As discussed above, landslides in Valles Marineris may also have important implications concerning water, and as such, have been extensively studied. Lucchitta (1978, 1979, 1987) described a few dozen wall rock landslides and postulated the involvement of water and seismic activity in slope failure based on morphologic and mobility evidence. Shaller *et al.* (1989) and Shaller & Komatsu (1994) compared the morphologies of Valles Marineris wall rock landslides to terrestrial landslides and concluded that some of the slides may have occurred under moist or wet conditions. A fluidized rheology with significant pore pressures achieved the best fit to Ophir Chasma wall rock landslide profiles in dynamic modelling performed by Harrison & Grimm (2003). In contrast, other workers utilized mobility statistics (McEwen 1989; Soukhovitskaya & Manga 2006) to argue that wall rock landslides behaved as dry materials. Bulmer & Zimmerman (2005) showed that some wall rock landslides may be a result of large- and small-scale gravitational failures spanning millions of years; their work further supported dry emplacement (McEwen 1989), but also implied the existence of recent ice in Valles Marineris. Qualitative and quantitative morphological evidence led Barnouin-Jha *et al.* (2005) to conclude that several wall rock landslides flowed by a basal glide mechanism and not as wet debris flows. Quantin *et al.* tabulated wall rock landslide morphology (2004a) and estimated landslide ages with impact crater statistics (2004b), but the studies were not conclusive with respect to the roles of fluids or seismicity in slope failure.

Through slope stability analysis, Clow & Moore (1988) determined that the walls of Valles Marineris consisted of rock rather than unlithified materials. Schultz (2002) and Caruso (2002) using similar, but more detailed approaches with higher resolution data, found that wall rock strengths are consistent with layered igneous rocks and ILD strengths are consistent with sedimentary or volcaniclastic rocks; furthermore, they gave evidence for seismic triggering of wall rock landslides. Previous studies have identified several flow-like mass wasting features in ILDs and invoked the involvement of fluids in their initiation and emplacement (Lucchitta 1990, 1996, 2001; Lucchitta & Rosanova 1997; Schultz 1998b; Skilling *et al.* 2002), but evidence linking the flows to specific main scarps or source areas remains elusive. This study has identified additional ILD slope failures including circular failures, several of which have been modelled. Our approach follows previous work on a Canadian analogue to the ILDs, where limit equilibrium analyses were used to determine the conditions at the time of failure for large landslides on a subglacial volcano (Neuffer *et al.* 2006). The slope failures were most likely triggered by the rapid drawdown of a surrounding englacial lake. Edifice collapse has been investigated in a similar manner on Cascade and Mexican volcanoes (e.g., Katzenstein & Watters 2003). Forster (2004) inquired as to whether a greater understanding of Martian geological processes could be gained by analysing large landslides on the planet. Through mapping and limit equilibrium back-analysis, this work shows that large landslides in the wall rock of Valles Marineris were most likely triggered by ground shaking, whereas slope failures in the ILDs could have been caused by gravity, fluid pressure, or ground shaking.

Approach

Mapping

Landslides in ILDs were mapped utilizing a Digital Elevation Model (DEM) and Viking, MOC (Mars Orbiter Camera), Mars Odyssey THEMIS (Thermal Emission Imaging System), and Mars Express HRSC (High Resolution Stereo Camera) satellite imagery. First, a custom DEM of the central Valles Marineris region was produced by the routine of Okubo *et al.* (2004). This method uses MOLA (Mars Orbiter Laser Altimeter) datasets in conjunction with GMT software to create 200 pixel/degree resolution DEMs of the Martian surface (Okubo *et al.* 2004). Next, the DEM was imported into GridView, which allows for the contouring and profiling of the topographic data. Possible slope failures were identified in GridView and verified by investigation of satellite imagery. From 65 possible landslides identified in the ILDs of central Valles Marineris, 11 landslides were confirmed (Fig. 1). Eight of the landslides initiated as circular failures as determined by the following criteria:

(i) Hummocky, convex, or lobate deposit
(ii) Concave, arcuate main scarp
(iii) No continuation of strata from deposit into intact adjacent slopes

Heights, lengths, and slope angles of selected landslides were measured on the DEM and are given in Table 1. Heights and lengths are defined as the vertical and horizontal distances between the main scarp and landslide toe (Cruden & Varnes 1996) along the

Fig. 1. Location of central Valles Marineris and studied landslides. Top image from MOLA topography. Bottom image from custom MOLA DEM. Approximate ILD mound boundaries in black. Yellow circles denote modelled landslides. Green squares show locations of other confirmed landslides.

Table 1. *Slope geometries and key modelling results for Valles Marineris landslides.*

Slide	Chasma	Unit	Section	H	L	α	RM	Water	r_u	pga	SF
1	Ophir	WR	Intact	8220	18080	24.4	Ba	dry	0.00	0.00	3.08
			West	8030	75770	6.0	Ba	dry	0.00	2.49	1.00
			East	8220	62710	7.5	Ba	art	0.69	0.00	1.00
							Ba	sat	sat	1.11	1.00
							DBa	dry	0.00	0.00	1.52
							DBa	dry	0.00	0.71	1.00
							DBa	art	0.41	0.00	1.00
							DBa	sat	sat	0.00	1.01
2	Hebes	WR	Intact	5370	15410	19.2	Ba	dry	0.00	0.00	4.43
			Slide	5060	49670	5.8	Ba	dry	0.00	3.24	1.00
							Ba	art	0.82	0.00	1.00
							Ba	sat	sat	1.80	1.00
							DBa	dry	0.00	0.00	2.20
							DBa	dry	0.00	1.24	1.00
							DBa	art	0.66	0.00	1.00
							DBa	sat	sat	0.54	1.00
3	Hebes	ILD	Intact	4640	14060	18.3	Sh	dry	0.00	0.00	0.55
			Slide	4280	13740	17.3	Ss	dry	0.00	0.00	2.17
							DSs	dry	0.00	0.00	0.77
							NT	dry	0.00	0.00	1.71
							DNT	dry	0.00	0.00	0.89
							HB	dry	0.00	0.00	3.68
							DHB	dry	0.00	0.00	2.29
							HF	dry	0.00	0.00	0.98
							WT	dry	0.00	0.00	1.08
							DWT	dry	0.00	0.00	0.21
4	Hebes	ILD	Slide	2350	5970	21.5	Sh	dry	0.00	0.00	0.44
							Ss	dry	0.00	0.00	1.80
							DSs	dry	0.00	0.00	0.59
							NT	dry	0.00	0.00	1.36
							DNT	dry	0.00	0.00	0.67
							HB	dry	0.00	0.00	3.16
							DHB	dry	0.00	0.00	1.88
							HF	dry	0.00	0.00	1.04
							WT	dry	0.00	0.00	0.89
5	E Candor	ILD	Slide	6450	33940	10.8	Sh	dry	0.00	0.00	0.43
							Ss	dry	0.00	0.00	1.76
							DSs	dry	0.00	0.00	0.57
							NT	dry	0.00	0.00	1.32
							DNT	dry	0.00	0.00	0.65
							HB	dry	0.00	0.00	3.09
							DHB	dry	0.00	0.00	1.83
							HF	dry	0.00	0.00	1.14
							WT	dry	0.00	0.00	0.87
6	E Candor	ILD	Slide	3470	24860	7.9	Sh	dry	0.00	0.00	0.92
							Ss	dry	0.00	0.00	3.73
							Ss	dry	0.00	1.71	1.00
							Ss	art	0.84	0.00	1.00
							Ss	sat	sat	1.08	1.00
							DSs	dry	0.00	0.00	1.28
							DSs	dry	0.00	0.19	1.00
							DSs	sat	0.33	0.00	1.00
							DSs	sat	sat	0.00	0.97
							NT	dry	0.00	0.00	2.91
							NT	dry	0.00	1.19	1.00
							NT	art	0.80	0.00	1.00
							NT	sat	sat	0.21	1.00
							DNT	dry	0.00	0.00	1.45

Table 1. *Continued.*

Slide	Chasma	Unit	Section	H	L	α	RM	Water	r_u	pga	SF
Key							DNT	dry	0.00	0.30	1.00
H: height (m)							DNT	*c*. sat	0.47	0.00	1.00
L: length (m)							DNT	*c*. sat	sat	0.00	1.00
α: slope angle (degrees)							HB	dry	0.00	0.00	6.47
RM: rock mass							HB	dry	0.00	3.27	1.00
r_u: fluid pressure/overburden pressure							HB	art	0.92	0.00	1.00
pga: peak horizontal ground acceleration (m/s^2)							HB	sat	sat	1.35	1.00
SF: Safety Factor							DHB	dry	0.00	0.00	3.94
WR: wall rock							DHB	dry	0.00	1.83	1.00
ILD: interior layered deposit							DHB	art	0.86	0.00	1.00
Ba: basalt							DHB	sat	sat	0.66	1.00
Sh: shale							HF	dry	0.00	0.00	1.99
Ss: sandstone							HF	dry	0.00	0.64	1.00
NT: nonwelded tuff							HF	*c*. sat	0.52	0.00	1.00
HB: hyaloclastite breccia							HF	*c*. sat	sat	0.00	1.00
HF: hyaloclastite fracture							WT	dry	0.00	0.00	1.87
WT: welded tuff							WT	dry	0.00	0.56	1.00
D (e.g., DBa): disturbed							WT	*c*. sat	0.60	0.00	1.00
art: artesian							WT	*c*. sat	sat	0.00	1.08
sat: fully saturated							DWT	dry	0.00	0.00	0.35

landslide centreline; slope angles are the arctangent of the height divided by the length.

Slope stability analysis

To evaluate the conditions at the time of landslide initiation in Valles Marineris, six slope failures were back-analyzed in 'Slide 5.0', a two-dimensional (2D) limit equilibrium analysis program produced by Rocscience Inc. Bishop's Simplified Method (Abramson *et al*. (2002)) and the Hoek–Brown failure criterion (Hoek *et al*. 2002) were used to model circular failure and material strengths, respectively. Two circular failure complexes in the Hebes and Ophir Chasmata (Slides 1 and 2) (Fig. 1, Table 1) were chosen to evaluate failure mechanisms in the wall rock of Valles Marineris. Four circular failures in the ILD were selected for slope stability modelling in the Hebes and East Candor Chasmata (Slides 3–6) (Fig. 1, Table 1). Pre-failure slope geometries were estimated by one of two methods:

(i) Where multiple failure episodes (Slides 1 and 2) or landslide deposit erosion (Slide 3) were significant, profiles of adjacent intact slopes were imported directly into 'Slide 5.0' (Figs. 2 & 3). The intact profile used for Slide 2 was truncated at an elevation of −1700 m to account for an ILD bench that underlies the landslide, but not the intact slope (Fig. 3).

(ii) Where multiple failure episodes or landslide deposit erosion were not significant (Slides 4–6), the original slope profile was estimated by area balancing (a 2D approximation of volume balancing): the areas of the two polygons created by the superposition of an estimated pre-failure profile on the current, failed slope profile were balanced by inspection. The estimated profile mimicked the curvature of adjacent intact slopes.

While the two methods are different in approach, and volume balancing may not always be appropriate (e.g. material entrainment, bulk density changes during emplacement), the models are not overly sensitive to slope geometry: Slide 3 was analysed with initial slope geometries from both methods and the resulting safety factors varied by less than 15%.

The unit weights of slope materials and water were adjusted to account for Martian gravity, which is *c.* 38% of Earth's gravity. Because rock strengths have not been directly measured on Mars, this study substituted minimum terrestrial rock mass strengths for analogous Martian deposits. The rock engineering and engineering geology literature were searched for the lowest Hoek–Brown strength parameters for clastic sedimentary, tuff, hyaloclastite (product of subaqueous/subice volcanism), basalt, and mafic intrusive rock masses, which were then used in the models with appropriate candidate lithologies (Table 2). The Hoek–Brown criterion is a nonlinear, semi-empirical rock mass strength criterion that accounts for the fractured nature of rock masses by incorporating rock mass classifications such as the Geological Strength Index (GSI). Due to the lack of published strength data for hyaloclastite, Mohr–Coulomb strength parameters determined by direct shear testing of fracture surfaces in hyaloclastite breccia (Neuffer *et al*. 2006) were also utilized as minimum rock mass

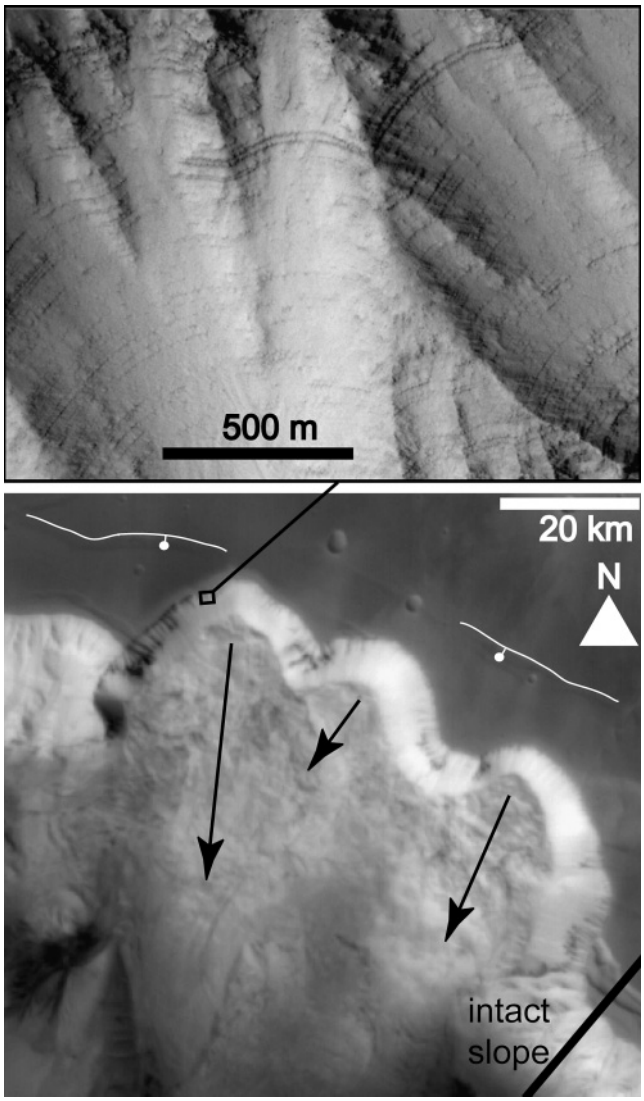

Fig. 2. (a) Ophir Chasma wall rock landslide complex (Slide 1) and detail of wall rock (illumination from left). Black arrows indicate landslide movement direction. White lines show normal faults with ball on downthrown side. Images modified from MOC Images R0900883 and R0902007.

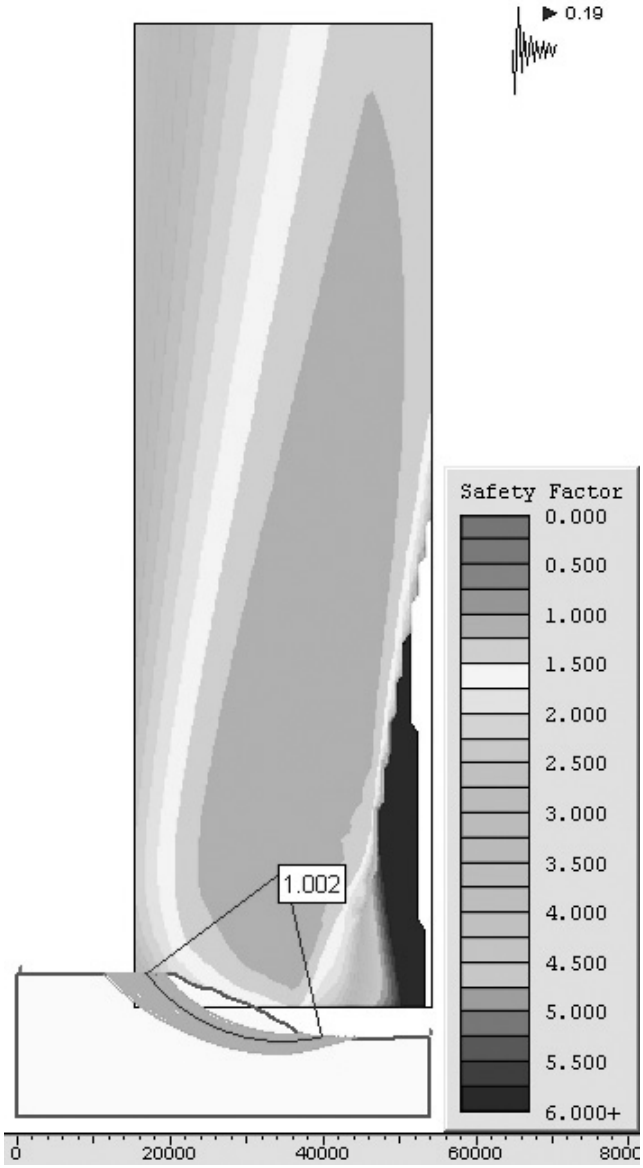

Fig. 2. (b) Sample model result for Slide 1. Rock mass is dry, disturbed basalt and seismic load is 0.19 Mars g. Dark grey and light grey curves are the most critical and 100 most critical slip surfaces, respectively. Scale is 1:1 and in metres.

strengths (Lockner 1995) (Table 2). Minimum terrestrial rock mass strengths should be lower than corresponding Martian strengths due to the reduced influence of water on rock weathering and alteration on Mars. The use of minimum rock mass strengths allowed for the influences of fluid pressure and seismic loading to be reliably evaluated, as cases where modelled slopes did not fail under dry, static, minimum strength conditions indicated that an additional triggering factor was necessary for landslide initiation. Thus, the calculated fluid pressures or seismic loads are the minimum values needed to cause slope failure. However, because minimum rock mass strengths were used, seismic loading or fluid pressure cannot be ruled out for slopes that did not require an additional triggering mechanism for failure, as the Martian rock masses are most likely stronger than those used in the models. The disturbance factor (Hoek *et al.* 2002) was varied from 0 (undisturbed) to 1 (disturbed), as rock masses in Valles Marineris may be disturbed by impacts or exhumation.

Fluid pressure in the slopes was assumed to be hydrostatic, and was simulated by back-analysis for the r_u coefficient (ratio of fluid pressure to overburden pressure) and potentiometric surface location required for failure. For landslides in Valles Marineris, impacts, in addition to faults, must be considered as sources of ground acceleration. Both types of seismic loading were modelled as pseudostatic, horizontal ground accelerations. To determine the ground acceleration at a slope from a given fault rupture, empirical methods were utilized. First, the approximate surface trace length of the fault was measured on the DEM, and used in a

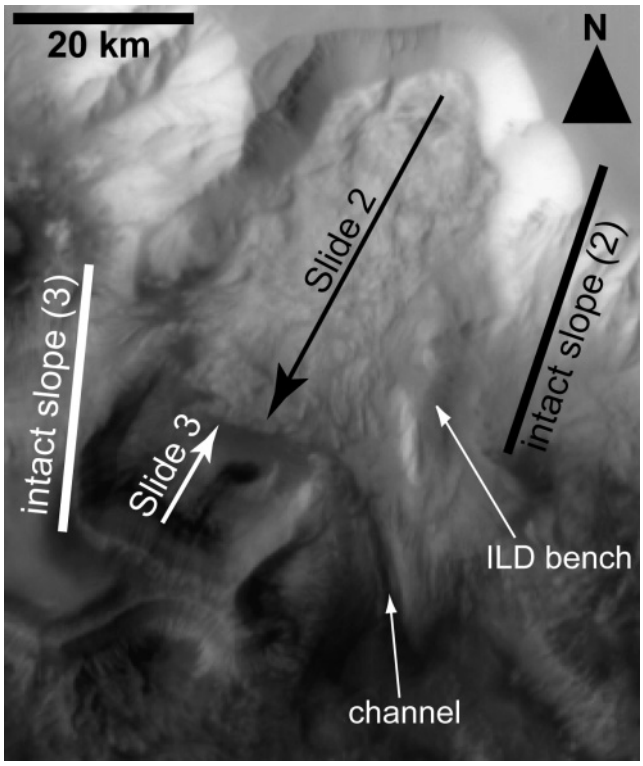

Fig. 3. (a) Hebes Chasma wall rock landslide complex (Slide 2) and ILD landslide (Slide 3). Arrows show movement directions for respective landslides. Image modified from MOC Image R0301338. Illumination from left.

correlation by Wells & Coppersmith (1994) to calculate the magnitude of a Marsquake on the fault. Next, the peak ground acceleration at the slope was estimated by plugging the magnitude and distance between the slope base and fault trace into an empirical formula from Joyner & Boore (1981). The ground acceleration at a slope caused by an impact was estimated following the methods of Chuang & Greeley (2000). First, horizontal ground force was determined by equations relating the ground force produced by an impact to crater diameter and distance from the source, in this case, the distance between the slope base and crater edge. Next, horizontal ground acceleration from the impact was calculated by multiplying the ground force by the landslide mass. Landslide mass was computed from the unit weight for the corresponding rock mass (Table 2) and landslide volume estimates from Harrison & Grimm (2003) and Quantin *et al*. (2004a). The volume of Slide 6 (*c*.10 km^3) was estimated from the DEM. Because the volume estimates are for the entire slide mass, the results are representative of the ground force necessary to cause slope failure in a single episode; landslides that failed in multiple episodes may have been triggered by smaller or more distant impacts. Impact craters more than 200 km away from a landslide were not considered due to limitations in the ground force estimation method (Chuang & Greeley 2000).

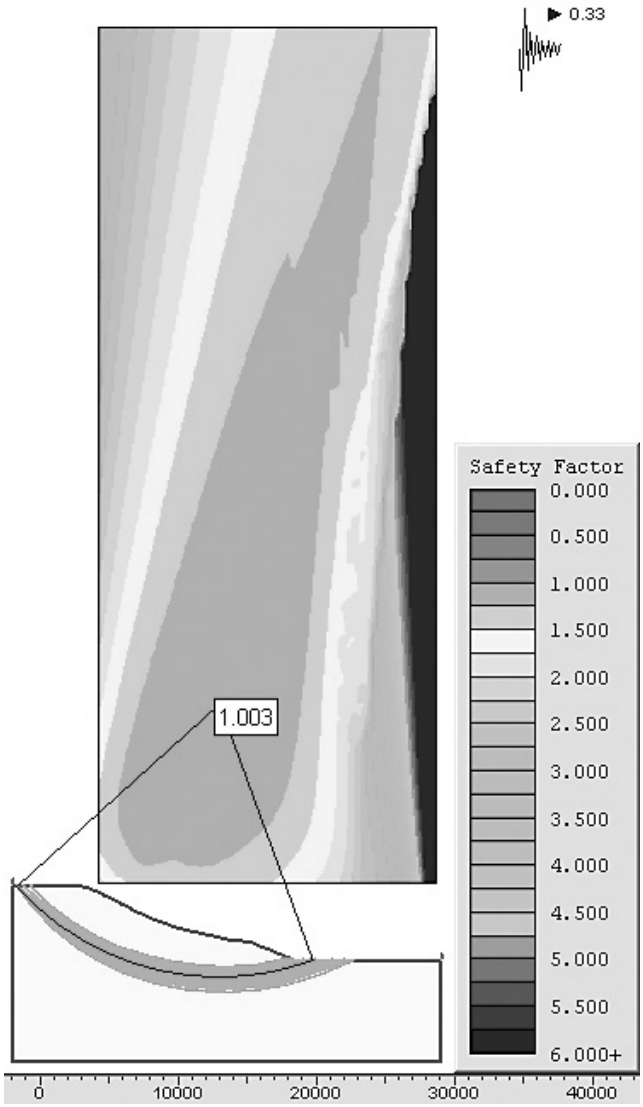

Fig. 3. (b) Sample model result for Slide 2. Rock mass is dry, disturbed basalt and seismic load is 0.33 Mars g. Dark grey and light grey curves are the most critical and 100 most critical slip surfaces, respectively. Scale is 1:1 and in metres.

Results

Nearly 140 scenarios were modelled with 'Slide 5.0'. Key results from the slope stability analyses are given in Table 1. The Ophir Chasma wall rock landslide complex (Slide 1) consists of three distinct landslides that display internal scarps and superposed flows, suggesting multiple failure episodes (Fig. 2a) (e.g. Barnouin-Jha *et al*. 2005). The west and east landslides are nearly equal in height to the adjacent intact slope used in modelling (Table 1). The centre landslide was not measured due to uncertainty in the location of the slide toe, but inspection of the DEM suggests a similar height to the west and east landslides (Fig. 1). Hence, the slope stability model approximates failure for all three landslides. The Ophir Chasma landslide complex required additional triggering mechanisms, given basalt rock mass strengths

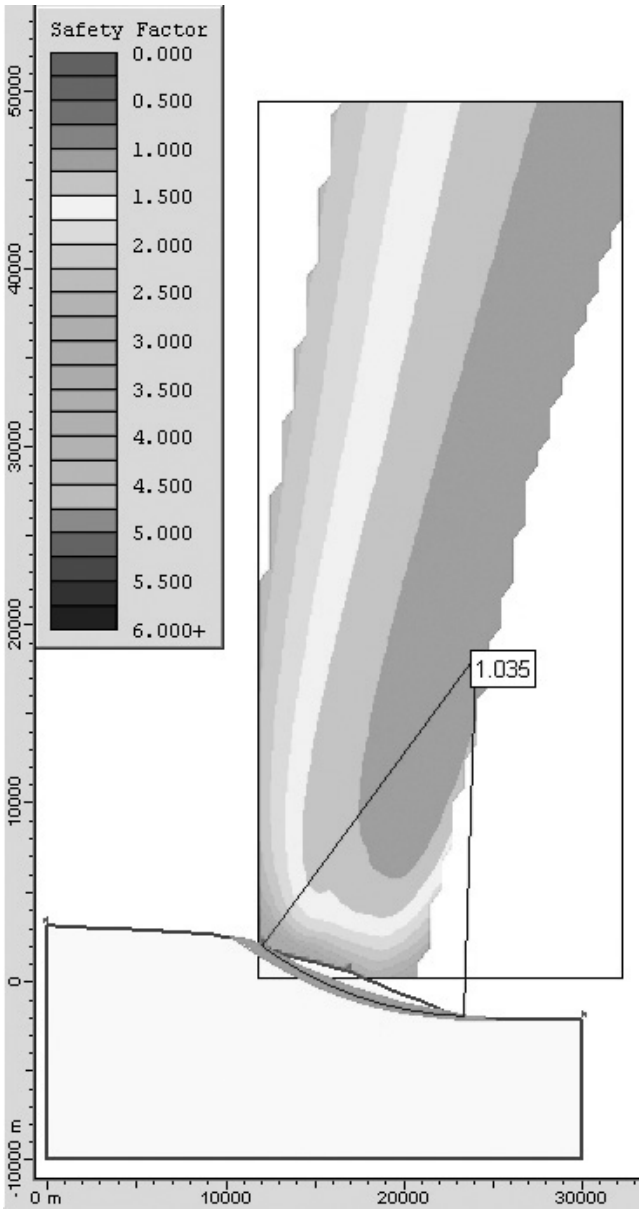

Fig. 3. (c) Sample model result for Slide 3. Rock mass is represented by the dry, hyaloclastite fracture strength. Dark grey and light grey curves are the most critical and 100 most critical slip surfaces, respectively.

(Table 1, Fig. 2b). Fluid pressures equal to 41% and 69% of overburden pressure were required for the failure of disturbed and undisturbed basalt rock masses, respectively (Table 1). For the initial slope, an r_u value of 0.41 roughly corresponds to a fully saturated rock mass (Table 1). Alternatively, ground accelerations of 0.19 and 0.67 Mars *g* resulted in failure of disturbed and undisturbed, dry basalt rock masses, respectively (Table 1, Fig. 2b). Nearby impact craters could not have generated the required ground accelerations for the individual slide masses, but two normal faults on the plateau surface (Fig. 2a), or any unidentified fault 1.5 km or longer within 0.5 km of the landslides could have produced the ground shaking (3.7–4.5 m/s^2 and 2.5 m/s^2, respectively) necessary for the failure of disturbed or undisturbed rock masses (Table 1).

The Hebes Chasma wall rock landslide complex (Slide 2) has numerous internal scarps indicative of multiple failure episodes or differential movement of the slide mass (Fig. 3a). Slide 2 overlies ILDs and terminates in the partially evacuated scarp of an ILD landslide (Slide 3) (Fig. 3a). Given basalt rock mass strengths, Slide 2 required an additional triggering mechanism (Table 1, Fig. 3b). Artesian fluid pressures equal to 66% and 82% of overburden pressure were required for the failure of disturbed and undisturbed basalt rock masses, respectively (Table 1). Alternatively, ground accelerations of 0.33 and 0.87 Mars *g* resulted in failure of disturbed and undisturbed, dry basalt rock masses, respectively (Table 1, Fig. 3b). For a disturbed rock mass, the large impact crater on the plateau to the south of Hebes Chasma (Fig.1), or any unidentified fault 1000 m or longer within 500 m of the landslide could have readily produced the ground shaking (2.7 m/s^2 and 2.3 m/s^2, respectively) necessary for slope failure (Table 1). For an undisturbed rock mass, any unidentified fault 3.5 km or longer within 0.5 km of the landslide could have generated the required ground acceleration (3.2 m/s^2) (Table 1).

The deposit of Slide 3 in the Hebes Chasma ILD has been partially removed and a dark material that may be lava (Ori *et al.* 2005) has flowed down the scarp (Fig. 3a). The deposits of Slides 4 and 5 in the ILDs of the Hebes and East Candor Chasmata are largely intact, although fluting on the toes suggests minor wind erosion (Figs. 4a & 5a). The scarps of Slides 3–5 are fluted (Figs. 3a, 4a & 5a) implying that the bulk of the failed material is erodible by wind, and, hence, probably better represented by the sedimentary, nonwelded tuff, and hyaloclastite strengths than the welded tuff and basalt strengths. Slope stability modelling indicated that Slides 3–5 could have failed under dry, static conditions for the shale, disturbed sandstone, disturbed nonwelded tuff, and welded tuff rock mass strengths (Table 1). In addition, the hyaloclastite fracture strength resulted in failure for Slide 4 (Fig. 4b) and nearly resulted failure for Slides 3 (Fig. 3c) and 5 for dry, static conditions (Table 1). If the ILD rock masses comprising the failed slopes were stronger than the representative strengths, or consisted of hyaloclastite breccia similar in strength to the terrestrial example, water or ground shaking would have been involved in landslide initiation.

Slide 6 in the East Candor Chasma ILD shows a well-defined scarp that steps down through light to intermediate albedo beds (Fig. 6a). The fluted, fan-shaped deposit has numerous knobs or boulders up to *c.* 200 m in diameter on the deposit surface (Fig. 6a). Slide 6 could have failed under dry, static conditions for the shale and disturbed welded tuff rock masses only (Table 1). While simple gravitational failure cannot be ruled out for the above strengths, the results suggest an additional triggering mechanism acted on the slope if strengths are

Table 2. *Minimum terrestrial rock mass strengths used in slope stability modelling.*

Rock Mass	GSI	UCS (MPa)	m_i	φ	c (MPa)	γ (kN/m^3)	Source
Shale	10	11	4			10.1	Dalgic 2000
Sandstone	30	25	18			10.1	Hoek *et al.* 1998
Nonwelded Tuff	55	6	8			5.4	Aydan & Ulusay 2003
Hyaloclastite Breccia	60	24	18			6.1	Neuffer *et al.* 2006
Hyaloclastite Fracture				18	0.11	6.1	Neuffer *et al.* 2006
Welded Tuff	12	12	10			6.8	Ozsan & Basarir 2003
Basalt	43	142	25			9.1	Ozsan & Basarir 2003
Gabbro	63	96	27			11.3	Wines & Lilly 2001

GSI: Geologic Strength Index (Hoek & Brown 1997)
UCS: Uniaxial Compressive Strength for intact rock
m_i: material constant for intact rock (Hoek *et al.* 2002)
φ friction angle
c: cohesion
γ: unit weight

better represented by the sandstone, nonwelded tuff, or hyaloclastite rock masses. Analyses showed that a Marsquake on the trough-bounding normal fault *c.* 20 km to the north (Fig. 6a) could have generated the ground acceleration (1.1–1.9 m/s^2) necessary to cause landsliding with the sandstone, nonwelded tuff, hyaloclastite fracture, disturbed hyaloclastite, and undisturbed welded tuff rock mass strengths (Table 1). Ground shaking (2.2–4.1 m/s^2) produced by the impact crater on the plateau surface *c.* 75 km northeast of the landslide (Fig. 1) could have caused failure for all viable rock mass strengths (Table 1). Alternatively, r_u values of 0.33–0.92 resulted in failure of the sandstone, nonwelded tuff, hyaloclastite, and undisturbed welded tuff rock masses (Table 1). These fluid pressure conditions correspond to approximately full saturation for the disturbed sandstone (Fig. 6b), disturbed nonwelded tuff, hyaloclastite fracture,

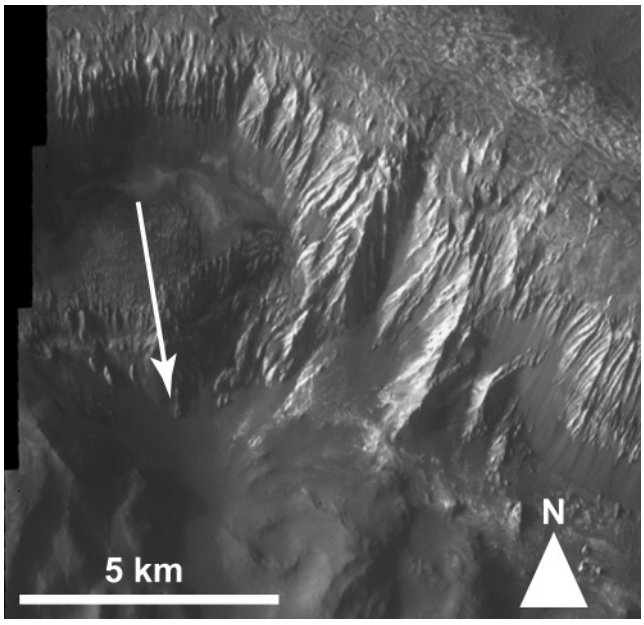

Fig. 4. (a) Hebes ILD landslide (Slide 4) and typical ILD morphology and stratigraphy (note dark cap unit at top right of the image). Arrow shows landslide movement direction. Edge at left of figure is the image edge. Image modified from THEMIS Visible Image V10988001. Illumination from left.

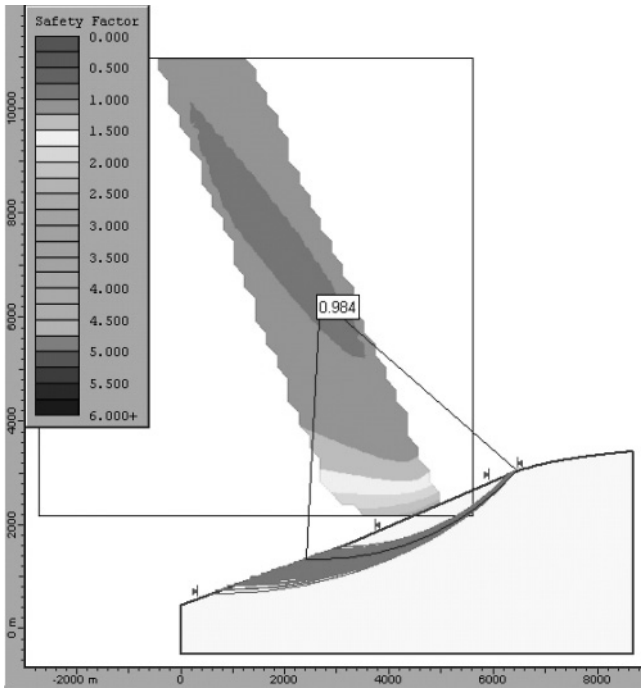

Fig. 4. (b) Sample model result for Slide 4. Rock mass is represented by the dry, hyaloclastite fracture strength. Dark grey and light grey curves are the most critical and 100 most critical slip surfaces, respectively.

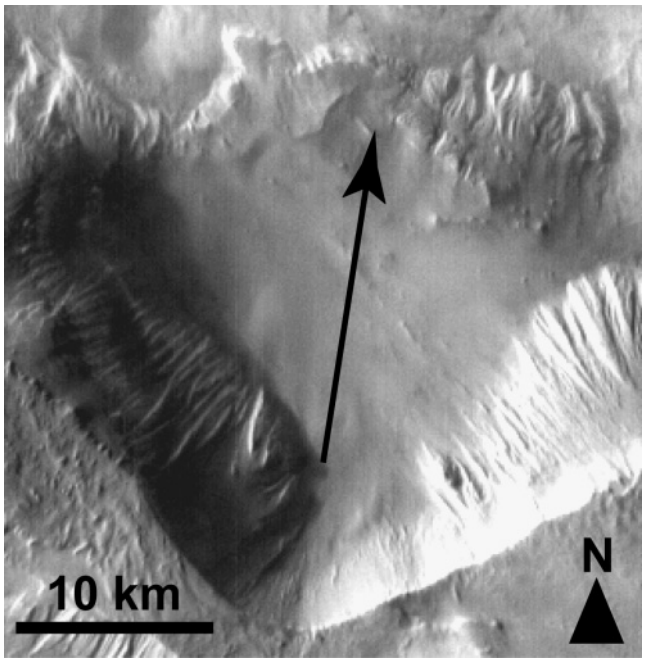

Fig. 5. (a) East Candor ILD landslide (Slide 5). Arrows shows landslide movement direction. Image modified from THEMIS Day Infared Image I10737006. Illumintation from left.

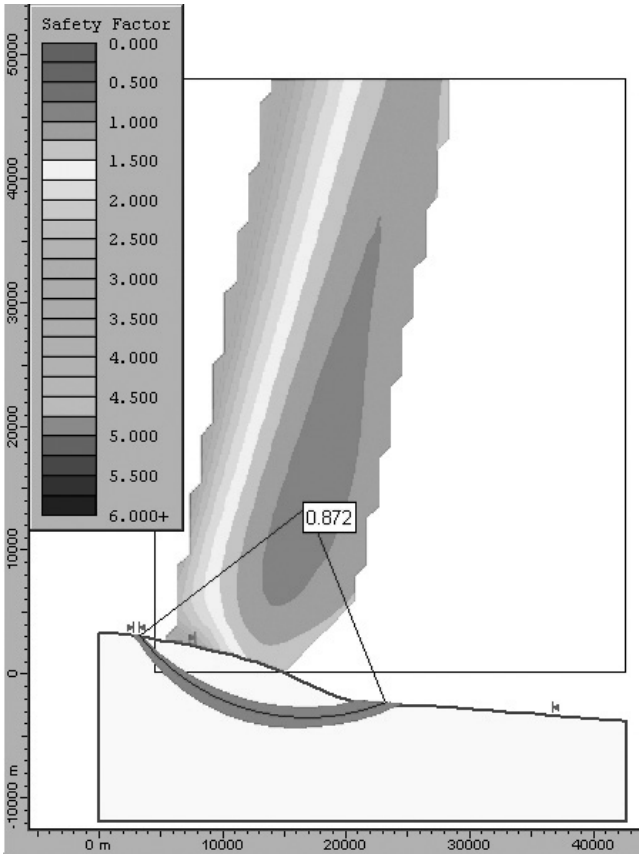

Fig. 5. (b) Sample model result for Slide 5. Rock mass is dry, welded tuff. Dark grey and light grey curves are the most critical and 100 most critical slip surfaces, respectively.

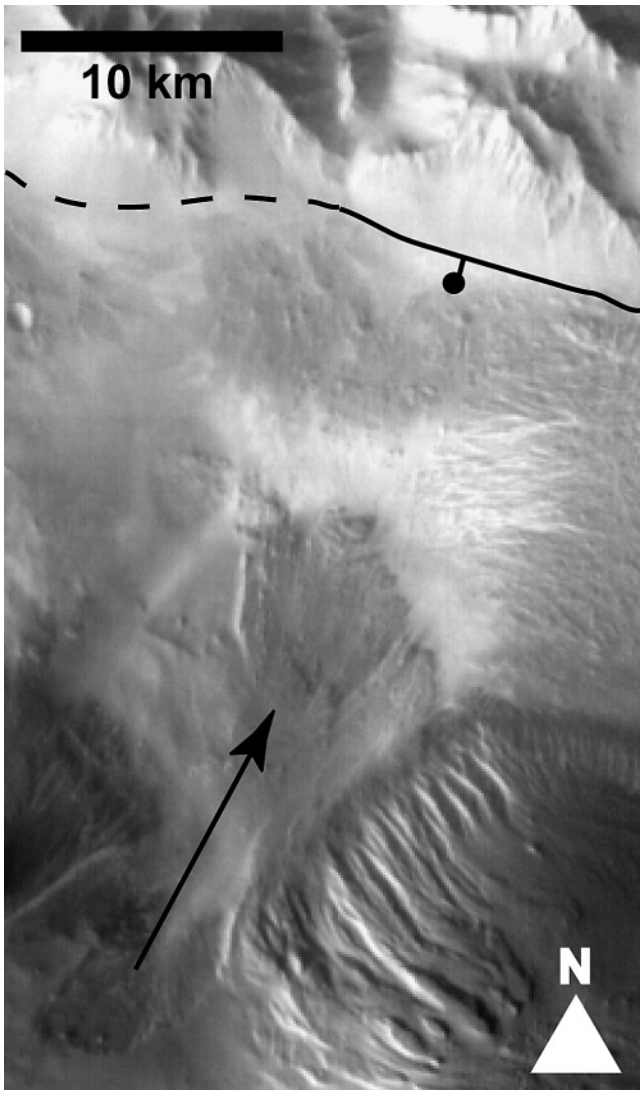

Fig. 6. (a) East Candor ILD landslide (Slide 6). Arrow shows landslide movement direction. Black line shows trough-bounding normal fault with ball on downthrown side. Image modified from THEMIS Day Infrared Image I107854024. Illumination from left.

and undisturbed welded tuff rock mass strengths or artesian pressures for the undisturbed sandstone, undisturbed nonwelded tuff, and hyaloclastite breccia rock mass strengths (Table 1).

Discussion

Liquid water is not currently stable at the surface of Mars, and calculations indicate that, where present, the cryosphere extends from several hundred metres below the surface to approximately 2 km depth at the Martian equator (Clifford 1993). While ground ice was not specifically modelled in this study, ice-filled fractures tend to increase the shear strength of a rock mass unless the temperature approaches the melting point (Davies *et al*. 2001); thus, excluding ground ice from the slope

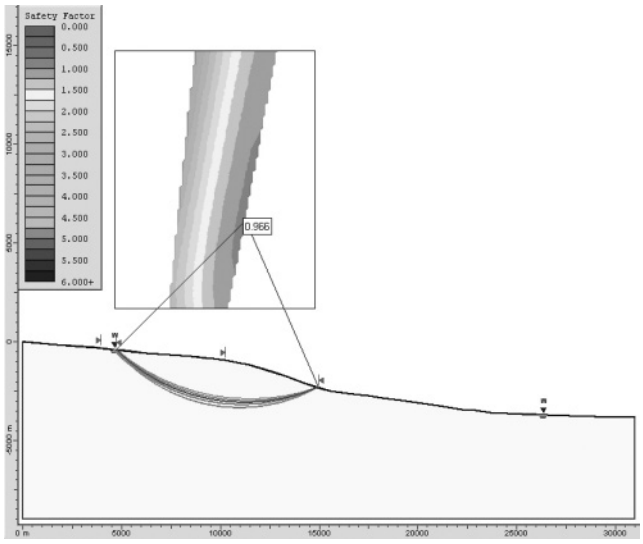

Fig. 6. (b) Sample model result for Slide 6. Rock mass is fully saturated, disturbed sandstone. Dark grey and light grey curves are the most critical and 100 most critical slip surfaces, respectively.

stability analyses is consistent with the use of minimum rock mass strengths. The fluid pressure analyses account for the scenario of ground ice reaching the melting point under possible, warmer past climates.

Under current conditions, slope failures resulting from fluids would necessarily involve confined aquifers beneath the cyrosphere. One problem with this scenario is the location of the wall rock landslides at regional topographic highs on the plateau (Fig. 1); recharge could originate from the Tharsis volcanic region to the west, but a low-lying area lies between Tharsis and the landslides (Fig. 1). However, faults could affect the distribution and pressures of fluids by enhancing along-strike rock mass permeability, decreasing cross-strike permeability, and inducing fluid pressure changes during slip events. It is not likely that Slide 6 failed as result of fluid pressure under current conditions, as the landslide is shallow and originated near the top of a rise (Fig. 6a). Volcanism in Valles Marineris is supported by observations (e.g. Lucchitta 1990; Chapman & Tanaka 2001) and a possible volcanic origin for ILDs. It is possible that elevated heat flow from volcanism in the trough system generated additional pore fluids in the wall rock and ILDs by melting the cryosphere.

Evidence for warmer and wetter episodes in Martian history is abundant (e.g. Jakosky & Mellon 2004; Baker 2001; Jakosky & Phillips 2001). As discussed above, the ILDs were most likely deposited beneath ice sheets or lakes that filled Valles Marineris. However, slope stability modelling indicates that, if fluids triggered Slides 1, 2, and 6, there were no water bodies buttressing the slopes at failure. This is further supported by the superposition of Slides 1 and 2 (Fig. 3a) and most other wall rock landslides on ILDs. Hence, for Slide 1, the fluid pressures required for failure would have been derived from confined aquifers or the rapid and complete drawdown of a surrounding lake. Rapid drawdown is an unlikely failure scenario, as DEM analyses indicate that putative lake surfaces in the Ophir, Candor, and Coprates Chasmata (Fig. 1) could only reach levels of -4300 m, -3050 m, and -3650 m, respectively before breaching into adjacent depressions. These elevations require a very high temporary dam (e.g. ice) to achieve the lake level of *c.* 3500 m necessary to saturate the Ophir Chasma wall rock and do not allow for the complete, rapid drawdown of a lake in Ophir Chasma. For Slide 2, the fluid pressures necessary for failure could only have been derived from a confined aquifer. If Slide 6 was triggered by fluids during a warmer climate, the fluid pressures could have been derived from aquifers within the ILD or the complete, rapid drawdown of a surrounding lake (Fig. 6b). Rapid drawdown is consistent with a subglacial (e.g. Skilling 1994; Neuffer *et al.* 2006) or local ice-dammed lake environment for East Candor Chasma. The topographic limitations discussed above for Ophir Chasma do not apply to Slide 6 because a body of ice in East Candor Chasma could produce an englacial or intraglacial lake with an elevation of *c.* -300 m necessary to saturate the pre-failure slope; drainage of this relatively small lake could be accommodated by flow into depressions west of the landslide (Fig. 1). Complete, rapid drawdown produces pore pressures approximately equivalent to a fully saturated rock mass (Walker & Santi 2004; Neuffer *et al.* 2006). Near or total saturation of the pre-failure slope for Slide 6 causes failure for the same rock mass strengths that failed under dry conditions for the other three ILD landslides (Slides 3–5) (Table 1). Additionally, if higher (MOC) resolution images show that the knobs on the deposit of Slide 6 are boulders, the landslide may have been emplaced as an energetic, turbulent, debris flow (e.g. Barnouin-Jha *et al.* 2005) implying the involvement of water.

A notch eroded in a wall rock spur downhill from the Ophir landslide deposits (Lucchitta 1987) and a steep channel in the ILDs downstream from the Hebes Chasma wall rock landslide deposit (Fig. 3a) are indirect evidence for water in the landslides, although both features could have other origins. Interestingly, the pore pressures necessary for failure of basaltic wall rock in Ophir Chasma are comparable to the pore pressures required for the initiation and runout of the west and east landslides of the Slide 1 complex (Fig. 2a). Assuming the landslides failed in single episodes, Harrison & Grimm (2003) predicted r_u values of 0.49 and 0.35 for the general fluidization rheology which best fit the western and eastern landslide deposits, respectively; this study calculated an r_u value of 0.41 (Table 1) for landslide initiation in a disturbed, basalt rock mass. Harrison & Grimm (2003) point out that their required fluid pressures needed to exist only at the base of the landslide; accordingly, ground shaking could have initi-

ated the wall rock landslides and a relatively small volume of interstitial fluids could have caused a fluidized rheology and possibly fluvial erosion downstream.

Indeed, while seismic loading and the presence of fluids are not mutually exclusive (Table 1), this study shows that fluids are not required for the failure of the modelled landslides in Valles Marineris. With numerous, unambiguous signs of recent faulting and impacts in and around the trough system, ground shaking is the most probable triggering agent for landslides in Valles Marineris. In addition, the most critical failure surfaces from the seismic loading models of Slides 1 and 2 more closely matched the actual failure geometries as they involved the entire slope height with no user-imposed limits on scarp and toe location (Figs. 2b & 3b). On the other hand, the fluid pressure models of Slides 1 and 2 required artificial limits on slip surface location to incorporate the entire slope height in the most critical failure surface. Furthermore, in addition to the above-mentioned difficulty of generating artesian pressures at a regional topographic high, there is no evidence for fluid breakout on the scarps of Slides 1, 2, and 6: failure of a slope due to artesian pressures would probably result in the massive release of fluids onto the landslide scarp and deposit. Hence, while a fluid pressure triggering mechanism cannot be ruled out, Slides 1 and 2 most likely failed as a result of fault-generated ground acceleration.

Slide 1 is among the highest and steepest wall rock failures in Valles Marineris while Slide 2 is roughly average in terms of initial slope dimensions (Table 1) (Harrison & Grimm 2003; Quantin *et al*. 2004a); as such, most wall rock landslides in Valles Marineris required triggering mechanisms and are not simple gravitational failures. Seismic loading is the most probable triggering mechanism for wall rock landslides, but fluid pressure cannot be ruled out, especially in regions of lower elevation where confined aquifers may be or may have been present. The four modelled ILD landslides represent a wide range of slope heights and angles (Table 1). None of the modelled ILD landslides required forces other than gravity to fail for minimum rock mass strengths, but triggering by fluids or ground shaking remains viable if rock masses were stronger than modelled. The landslide with the lowest slope angle (Slide 6) was most likely triggered by fluid pressure or seismic loading. Evidence of a specific triggering condition is needed to definitively state the failure mechanism for landslides in wall rock and ILDs. For example, a channel originating from a landslide scarp would strongly suggest failure due to artesian fluid pressures. Failure mechanisms may be further constrained by more accurately estimating material strengths: a consensus on the origin and lithology of the ILDs would narrow possible strengths; strength estimates for the ILDs and wall rock could be improved by higher resolution visible and spectral data to quantify fracture spacing and geometry, rock mass alteration, and lithological characteristics.

Conclusions

Landslides in the wall rock and ILDs of Valles Marineris, Mars were modelled using limit-equilibrium slope stability analysis to evaluate the mechanisms of slope failure. Eleven landslides, including eight circular failures, were mapped in the ILDs. Wall rock landslide complexes in the Ophir and Hebes Chasmata required artesian fluid pressures of at least 41% of overburden pressure or ground accelerations of at least 0.19 Mars *g* for failure. Agreement between modelled and observed failure surface geometries and the difficulty of generating artesian pressures at a regional topographic high indicate that ground shaking from Marsquakes or impacts most likely triggered the modelled wall rock landslides. Triggering mechanisms, such as ground acceleration or fluid pressure, were also necessary for most other landslides in Valles Marineris wall rock. Given minimum rock mass strengths, ILD landslides in the Hebes and East Candor Chasmata did not require triggering mechanisms; thus, landslides in ILDs may be a result of gravitational, fluid, or seismic loading.

Acknowledgements. Support for this study was provided by the Planetary Geology and Geophysics Program of the National Aeronautics and Space Administration. The authors thank G. Komatsu (International Research School of Planetary Sciences), M. Chapman (U.S. Geological Survey), R. Watters (University of Nevada, Reno), J. Daemen (University of Nevada, Reno), and an anonymous referee for insightful comments which improved this work. D.N. thanks C. Neuffer for help with the reference list and proofreading.

References

Abramson, L.W., Lee, T.S., Sharma, S. & Boyce, G.M. 2002. *Slope Stability and Stabilization Methods.* John Wiley & Sons, New York.

Allen, C.C., Jercinovic, M.J. & Allen, J.S.B. 1982. Subglacial volcanism in north-central British Columbia and Iceland. *Journal of Geology,* **90**, 699–715.

Aydan, A. & Ulusay, R. 2003. Geotechnical and geoenvironmental characteristics of man-made underground structures in Cappadocia, Turkey. *Engineering Geology,* **69**, 245–272.

Baker, V.R. 2001. Water and the martian landscape. *Nature,* **412**, 228–236.

Barnouin-Jha, O.S., Baloga, S. & Glaze, L. 2005. Comparing landslides to fluidized crater ejecta on Mars. *Journal of Geophysical Research,* **110**, E04010–doi: 10.1029/2003JE002214.

Bulmer, M.H. & Zimmerman, B.A. 2005. Reassessing landslide deformation in Ganges Chasma, Mars. *Geophysical Research Letters,* **32**, L06201–doi: 10.1029/2004GL022021.

CARUSO, P.A. 2002. *Seismic Triggering of Martian Landslides and Slope Stability for Valles Marineris, Mars.* M.S. thesis. University of Nevada, Reno.

CHAPMAN, M.G. & TANAKA, K.L. 2001. Interior trough deposits on Mars: subice volcanoes? *Journal of Geophysical Research,* **106**, 10087–10100.

CHUANG, F.V. & GREELEY, R. 2000. Large mass movements on Callisto. *Journal of Geophysical Research,* **105**, 20227–20244.

CLIFFORD, S.M. 1993. A model for the hydrologic and climatic behavior of water on Mars. *Journal of Geophysical Research,* **98**, 10973–11016.

CLOW, G.D. & MOORE, H.J. 1988. Stability of chasma walls in the Valles Marineris, Mars. *Lunar and Planetary Science Conference Abstracts,* **19**, 201–202.

CROFT, S.K. 1990. Geologic map of the Hebes Chasma quadrangle. *VM500K 00077 (abstract).* NASA-TM. 4210, 539–541.

CRUDEN, D.M. & VARNES, D.J. 1996. Landslide types and processes. *In:* TURNER, A.K. & SCHUSTER, R.L. (eds) *Landslides: Investigation and Mitigation.* Special Report, **247**. Transportation Research Board, National Academy Press, Washington D.C., 36–75.

DALGIC, S. 2000. The influence of weak rocks on excavation and support of the Beykoz Tunnel, Turkey. *Engineering Geology,* **58**, 137–148.

DAVIES, M.C.R., HAMZA, O. & HARRIS, C. 2001. The effect of rise in mean annual temperature on the stability of rock slopes containing ice-filled discontinuities. *Permafrost and Periglacial Processes,* **12**, 137–144.

FORSTER, A. 2004. Is there a role for engineering geology on Mars? *Quarterly Journal of Engineering Geology and Hydrogeology,* **37**, 5–6.

FUETEN, F., STESKY, R.M. & MACKINNON, P. 2005*a*. Structural attitudes of large scale layering in Valles Marineris, Mars, calculated from Mars Orbiter Laser Altimeter data and Mars Orbiter Camera imagery. *Icarus,* **175**, 68–77.

FUETEN, F., STESKY, R. & HRSC CO-INVESTIGATOR TEAM *ET AL.* 2005*b*. Attitude determination of geological layers using HRSC data and Orion software. *Lunar and Planetary Science Conference Abstracts,* **36**, 1498.

GUDMUNDSSON, M.T., SIGMUNDSSON, F. & BJÖRNSSON, H. 1997. Ice-volcano interaction of the 1996 Gjálp subglacial eruption, Vatnajökull, Iceland. *Nature,* **389**, 954–957.

HARRISON, K.P. & GRIMM, R.E. 2003. Rheological constraints on Martian landslides. *Icarus,* **163**, 347–362.

HAUBER, E., GWINNER, K. & HRSC CO-INVESTIGATOR TEAM *ET AL.* 2005. Interior layered deposits in Valles Marineris. Mars: insights from 3D-data obtained by the High Resolution Stereo Camera (HRSC). *Lunar and Planetary Science Conference Abstracts,* **36**, 1760.

HICKSON, C.J., MOORE, J.G., CALK, L. & METCALFE, P. 1995. Intraglacial volcanism in the Wells Gray – Clearwater volcanic field, east-central British Columbia, Canada. *Canadian Journal of Earth Sciences,* **32**, 838–851.

HOEK, E. & BROWN, E.T. 1997. Practical estimates of rock mass strength. *International Journal of Rock Mechanics and Mining Sciences,* **34**, 1165–1186.

HOEK, E., MARINOS, P. & BENISSI, M. 1998. Applicability of the geological strength index (GSI) classification for very weak and sheared rock masses: the case of the Athens schist formation. *Bulletin of Engineering Geology and the Environment,* **57**, 151–160.

HOEK, E., CARRANZA-TORRES, C. & CORKUM, B. 2002. Hoek-Brown failure criterion. *Proceedings of the Fifth North American Rock Mechanics Symposium,* **1**, 267–273.

JAKOSKY, B.M. & PHILLIPS, R.J. 2001. Mars' volatile and climate history. *Nature,* **412**, 237–244.

JAKOSKY, B.M. & MELLON, M.T. 2004. Water on Mars. *Physics Today,* **57**, 71–76.

JONES, J.G. 1969. Intraglacial volcanoes of the Laugarvatn region, south-west Iceland—I. *Quarterly Journal of the Geological Society of London,* **124**, 197–211.

JOYNER, W.B. & BOORE, D.M. 1981. Peak horizontal acceleration and velocity from strong-motion records including records from the Imperial Valley, California, earthquake. *Bulletin of the Seismological Society of America,* **71**, 2011–2038.

KATZENSTEIN, K.W. & WATTERS, R.J. 2003. Abstract V51F-0337 *Influence of the geotechnical properties of dacite domes on the 1980 failure of Mt. St. Helens.* Eos Transactions, Fall Meeting Supplement 84. American Geophysical Union.

KOMATSU, G., GEISSLER, P.E., STROM, R.G. & SINGER, R.B. 1993. Stratigraphy and erosional landforms of layered deposits in Valles Marineris, Mars. *Journal of Geophysical Research,* **98**, 11105–11121.

KOMATSU, G., ORI, G.G., CIARCELLUTI, P. & LITASOV, Y.D. 2004. Interior layered deposits of Valles Marineris, Mars: analogous subice volcanism related to Baikal Rifting. Southern Siberia. *Planetary and Space Science,* **52**, 167–187.

LOCKNER, D.A. 1995. Rock failure. *In:* AHRENS, T.J. (ed.) *Rock Physics and Phase Relations: A Handbook of Physical Constants.* Reference Shelf 3. American Geophysical Union, 127–147.

LUCCHITTA, B.K. 1978. A large landslide on Mars. *Geological Society of America Bulletin,* **89**, 1601–1609.

LUCCHITTA, B.K. 1979. Landslides in Valles Marineris, Mars. *Journal of Geophysical Research,* **84**, 8097–8113.

LUCCHITTA, B.K. 1981. Valles Marineris-faults, volcanic rocks, channels, basin beds (abstract). *Reports of Planetary Geology Program.* NASA-TM. 84211, 419–421.

LUCCHITTA, B.K. 1982. Lakes or playas in Valles Marineris (abstract). *Reports on Planetary Geology Program.* NASA-TM. 85127, 233–234.

LUCCHITTA, B.K. 1987. Valles Marineris. *Mars: wet debris flows and ground ice. Icarus,* **72**, 411–429.

LUCCHITTA, B.K. 1990. Young volcanic deposits in the Valles Marineris, Mars? *Icarus,* **86**, 476–509.

LUCCHITTA, B.K. 1996. Young volcanism or extensive mass-wasting collapse inside West Candor Chasma, Mars. *Lunar and Planetary Science Conference Abstracts,* **27**, 779–780.

LUCCHITTA, B.K. 1999. *Geologic map of Ophir and Central Candor Chasmata (MTM-05072) of Mars 1:500,000 sheet.* Map I-2568, Miscellaneous Investigations Series. U.S. Geological Survey.

LUCCHITTA, B.K. 2001. Young dark mantles and light flows in Valles Marineris, Mars. *Lunar and Planetary Science Conference Abstracts,* **32**, 2059.

LUCCHITTA, B.K. 2004. A volcano composed of light-colored layered deposits on the floor of Valles Marineris. *Lunar and Planetary Science Conference Abstracts,* **35**, 1881.

LUCCHITTA, B.K. & ROSANOVA, C.E. 1997. Valles Marineris. Mars: volatiles in the interior deposits? *Lunar and Planetary Science Conference Abstracts,* **28**, 1512.

LUCCHITTA, B.K., ISBELL, N.K. & HOWLINGTON-KRAUS, A. 1994. Topography of Valles Marineris: implications for erosional and structural history. *Journal of Geophysical Research,* **99**, 3783–3798.

MALIN, M.C. & EDGETT, K.S. 2000. Sedimentary rocks of early Mars. *Science,* **290**, 1927–1937.

MATHEWS, W.H. 1947. "Tuyas," flat-topped volcanoes in northern British Columbia. *American Journal of Science,* **245**, 560–570.

McCauley, J.F. 1978. *Geologic map of the Coprates quadrangle of Mars 1:5,000,000 sheet.* Miscellaneous Investigations Series, Map I-897. U.S. Geological Survey.

McEwen, A.S. 1989. Mobility of large rock avalanches: evidence from Valles Marineris, Mars. *Geology,* **17**, 1111–1114.

McEwen, A.S., Malin, M.C., Carr, M.H. & Hartmann, W.K. 1999. Voluminous volcanism on early Mars revealed in Valles Marineris. *Letters to Nature.,* **397**, 584–586.

Nedell, S.S., Squyres, S.W. & Anderson, D.W. 1987. Origin and evolution of the layered deposits in the Valles Marineris, Mars. *Icarus,* **70**, 409–441.

Neuffer, D.P., Schultz, R.A. & Watters, R.J. 2006. Mechanisms of slope failure on Pyramid Mountain, a subglacial volcano in Wells Gray Provincial Park, British Columbia. *Canadian Journal of Earth Sciences,* **43**, 147–155.

Okubo, C.H., Schultz, R.A. & Stefanelli, G.S. 2004. Gridding Mars Orbiter Laser Altimeter data with GMT: effects of the pixel size and interpolation methods on DEM integrity. *Computers & Geosciences,* **30**, 59–72.

Ori, G.G., Pacifici, A., Komatsu, G.Neukum, G. & HRSC science team *et al.* 2005. A probable fluid lava flow in the Hebes Mensa (Mars) studied by HRSC images. *Lunar and Planetary Science Conference Abstracts,* **36**, 1648.

Ozsan, A. & Basarir, H. 2003. Support capacity estimation of a diversion tunnel in weak rock. *Engineering Geology,* **68**, 319–331.

Peterson, C. 1981. A secondary origin for the central plateau of Hebes Chasma. *Lunar and Planetary Science Conference Abstracts,* **12**, 1459–1471.

Quantin, C., Allemand, P. & Delacourt, C. 2004*a*. Morphology and geometry of Valles Marineris landslides. *Planetary and Space Science,* **52**, 1011–1022.

Quantin, C., Allemand, P., Mangold, N. & Delacourt, C. 2004*b*. Ages of Valles Marineris (Mars) landslides and implications for canyon history. *Icarus,* **172**, 555–572.

Schultz, R.A. 1998*a*. Multiple-process origin of Valles Marineris basins and troughs, Mars. *Planetary Space Science,* **46**, 827–834.

Schultz, R.A. 1998*b*. *Geologic Map of the Western Ophir Planum Region (MTM-10067) of Mars 1:500,000 sheet.* Miscellaneous Investigations Series, Map I-2588. U.S. Geological Survey.

Schultz, R.A. 2002. Stability of rock slopes in Valles Marineris, Mars. *Geophysical Research Letters,* **29**, 19, 1932–doi: 10.1029/2002GL015728.

Shaller, P.J. & Komatsu, G. 1994. Landslides on Mars. *Landslide News,* **8**, 18–22.

Shaller, P.J., Murray, B.C. & Albee, A.L. 1989. Subaqueous landslides on Mars? *Lunar and Planetary Science Conference Abstracts,* **20**, 990–991.

Sharp, R.P. 1973. Mars: troughed terrain. *Journal of Geophysical Research,* **78**, 4068–4072.

Skilling, I.P. 1994. Evolution of an englacial volcano: Brown Bluff, Antarctica. *Bulletin of Volcanology,* **56**, 573–591.

Skilling, I.P., Chapman, M.G. & Lucchitta, B.K. 2002. Young, blocky flows in East IUS/West Melas and West Candor Chasmata, Mars: debris avalanche deposits derived from Interior Layered Deposit (ILD) Mounds?. *Lunar and Planetary Science Conference Abstracts,* **33**, 1361.

Smellie, J.L., Hole, M.J. & Nell, P.A.R. 1993. Late Miocene valley-confined subglacial volcanism in northern Alexander Island, Antarctic Peninsula. *Bulletin of Volcanology,* **55**, 273–288.

Soukhovitskaya, V. & Manga, M. 2006. Martian landslides in Valles Marineris: wet or dry? *Icarus,* **180**, 348–352.

van Bemmelen, R.W. & Rutten, M.G. 1955. *Tablemountains of Northern Iceland.* E.J. Brill, Leiden, Netherlands.

Walker, S.R. & Santi, P.M. 2004. Influence of the Blue Mesa Reservoir on the Red Creek Landslide, Colorado. *Environmental and Engineering Geoscience,* **10**, 13–26.

Weitz, C.M. 1999. A volcanic origin for the interior layered deposits in Hebes Chasma, Mars. *Lunar and Planetary Science Conference Abstracts,* **30**, 1277.

Weitz, C.M. & Parker, T.J. 2000. New evidence that the Valles Marineris interior layered deposits formed in standing bodies of water. *Lunar and Planetary Science Conference Abstracts,* **31**, 1693.

Wells, D.L. & Coppersmith, K.L. 1994. New empirical relationships among magnitude, rupture length, rupture width, rupture area and surface displacement. *Bulletin of the Seismological Society of America,* **84**, 972–1002.

Werner, R. & Schmincke, H.U. 1999. Englacial vs. lacustrine origin of volcanic table mountains: evidence from Iceland. *Bulletin of Volcanology,* **60**, 335–354.

Wieczorek, G.F. 1996. Landslide Triggering Mechanisms. *In:* Turner, A.K. & Schuster, R.L. (eds) *Landslides: Investigation and Mitigation.* Special Report, **247**. Transportation Research Board, National Academy Press, Washington D.C., 76–90.

Williams, J.P., Paige, D.A. & Manning, C.E. 2003. Layering in the wall rock of Valles Marineris: intrusive and extrusive magmatism. *Geophysical Research Letters,* **30**, 12, 1623–doi: 10.1029/2003GL017662.

Wines, D.R. & Lilly, P.A. 2001. A comparative analysis of rock mass classification schemes in part of the Fimiston Open Pit Operation in Kalgoorlie, Western Australia. *Australian Geomechanics,* **36**(4), 59–72.

Witbeck, N.E., Tanaka, K.T. & Scott, D.H. 1991. *Geologic Map of the Valles Marineris Region, Mars (east and west half) 2-1:2,000,000 sheets.* Map I-2010. Miscellaneous Investigations Series. U.S. Geological Survey.

Received 25 August 2005; accepted 20 January 2006.